Binderless Composite Electrode Monolith from Carbon Nanotube and Biomass Carbon Activated by H_2SO_4 and CO_2 Gas for Supercapacitor

M. Deraman[1,*], M. M. Ishak[1], R. Farma[1,2], Awitdrus[1,2], E. Taer[1,2], I. A. Talib[1], and R. Omar[1]

[1]*School of Applied Physics, Faculty of Science and Technology, Universiti Kebangsaan Malaysia, 43600 Bangi, Selangor, Malaysia*

[2]*Department of Physics, Faculty of Mathematics and Natural Sciences, University of Riau, 28293 Pekanbaru, Riau, Indonesia*

**Email: madra@pkrisc.cc.ukm.my*

Abstract. Binderless composite electrodes in the monolithic form prepared from carbon nanotubes (CNTs) and self-adhesive carbon grains (SACG) from fibers of oil palm empty fruit bunch were studied as an electrode in a supercapacitor. The green monoliths (GMs) were prepared from three different types of precursors, SACG, SACG treated with 0.4 Molar H_2SO_4 and mixture of SACG and 5% CNTs (by weight) treated with 0.4 Molar H_2SO_4, respectively. These GMs were carbonized at 600°C in N_2 gas environment and activated by CO_2 gas at 800°C for 1 hour to produce activated carbon monoliths (ACMs). The properties of the ACMs (density, porosity, microstructure, structure and electrical conductivity) were found affected by CNTs addition and acid treatment. The acid treatment did not improve the electrochemical behavior of the ACMs used as electrodes (specific capacitance, specific energy and specific power of the supercapacitor) in the supercapacitor cells but CNTs addition improves the equivalent series resistance of the cell.

Keywords: SACG, ACMs, CNT, supercapacitor, electrochemical behavior
PACS: 82.45.Gj, 82.45.Mp, 82.45.Wx, 82.47.Uv, 82.45.Fk, 82.80.Fk, 81.05.uj, 81.05.U-, 81.05.Rm

INTRODUCTION

Supercapacitors have the capability to store energy and deliver power within the range that can complement the function of batteries and dielectric capacitors. The energy comes from electrostatic charges that are stored at the electrode-electrolyte double layer interface. Activated carbon [1,2], metal - oxide [3,4] and electronically conducting polymer [5,6] are commonly used electrode materials in supercapacitors. Technological development of activated-carbon-based-supercapacitors has been steadily growing because of their low cost, large capacitance and long cycling life. High specific surface area offered by activated carbon contributes to the high specific capacitance of the supercapacitors. However, use of 100 % activated carbon produces electrodes with low electronic conductivity, causing a high energy or power loss during the charge and the discharge processes. Efforts to reduce this energy loss have been made by adding carbon nanotubes (CNTs) into activated carbon to produce composite electrodes since CNTs have high electronic conductivity [7,8]. Since CNTs has lower specific capacitance than activated carbon, the specific capacitance of the CNTs-activated-carbon composite electrodes has been improved by means of physical and chemical activations [9,10].

In the present paper we report the preparation and characterization of activated carbon monoliths (ACMs) electrodes from self-adhesive carbon grains (SACG) of fibers of oil palm empty fruit bunches (EFB). ACMs electrodes, label as ACM1, ACM2 and ACM3 were prepared from the green monoliths (GMs) of SACG, SACG treated with acid and a mixture containing 95 % (by weight) SACG and 5 % CNTs treated with acid, respectively. Physical activation using CO_2 gas was employed to produce ACMs. The ACMs were characterized to observe the effect of acid treatment and addition of CNTs on their density, electrical conductivity, porosity, microstructure and structure. The electrochemical characteristics of the ACMs electrodes used in the supercapacitors fabricated in this work and performance of these supercapacitors were investigated.

EXPERIMENTAL

Sample Preparation

Fibers of EFB were pre-carbonized at low temperature 280°C using our previous method [11], and

The 4th Nanoscience and Nanotechnology Symposium (NNS2011)
AIP Conf. Proc. 1415, 175-179 (2011); doi: 10.1063/1.3667250

followed by milling for 36 hours using a ball mill [AC Motor BS 500-11] to produce fine powder. The powder was sieved to produce the SACG with particle size less than 106 microns. 30 g of SACG and mixture of (95 % SACG + 5 % CNTs, by weight) were poured into 120 ml solution of H_2SO_4 acid at 0.4 Molar, respectively. The solution was stirred for 1 hour and followed by drying in oven at 100°C for 48 hours to produce dry powder. Furthermore the dried powder weighted at 10 g was milled for 20 minutes to obtain homogeneous powder. A press pelletizing machine (VISITEC 2009-Malaysia) with 250 $kgcm^{-2}$ of compression force was used to convert 0.75 g of the powder samples inside a mould with a diameter of 20 mm into the GMs.

Using our previous multi-step heating profile [11], the GMs were carbonized up to 600°C into carbon monoliths in a furnace (Vulcan Box Furnace 3-1750) under a 1.5 $l min^{-1}$ flow of N_2 gas. The carbon monoliths were activated at 800°C for 1 hour in a flow of 1.0 $l min^{-1}$ CO_2 gas with a heating rate of 5°Cmin^{-1} to produce ACMs. The ACMs produced were polished to a thickness of 0.4 mm. The polished ACMs, stainless steel 316L and H_2SO_4 (1 Molar) were used as electrodes, current collectors and electrolyte to fabricate symmetrical supercapacitors cells, respectively.

Characterization

The density of the GMs and ACMs were determined from the measurements of their weight (Mettler Toledo AB204) and dimension (Mitutoyo 193-253). The electrical conductivity of the ACMs was measured using a four-point-probe technique (Jandel Universal Probe & Keithley Micro-Ohmeter 220). The microstructures and morphology of the ACMs were investigated using a Field Emission Scanning Electron Microscope (FESEM) (Zeiss SUPRA 55VP). The X-ray diffraction (XRD) patterns of the ACMs were recorded from an X-ray diffractometer (Bruker AXS: model D8 Advance-$K_{\alpha 1}$ wavelength of 1.5406 Å). The porosity characteristics of the ACMs were investigated by nitrogen (77 K) adsorption-desorption isotherm experiments (ASAP 2010 Micromeritics).

The electrochemical characterization of the supercapacitor cells was carried out by galvanostatic charge-discharge (GCD), electrochemical impedance spectroscopy (EIS) and cyclic voltammetry (CV) methods (Solatron 1286 electrochemical interface). All the measurements were carried out at room temperature 25°C.

RESULTS AND DISCUSSION

The results in Table 1 show that GMs lost a lot of their weight and volume after being converted into ACMs; due to the release of non-carbon contents and rearrangement of carbon atoms during carbonization, respectively. A slight change in the density and a relatively larger change in the electrical conductivity of samples due to acid treatment and addition of CNTs are shown by the data in Table 1.

TABLE 1. Weight (w), diameter (d), thickness (t) and density (ρ) of GMs and ACMs, and electrical conductivity (σ) of ACMs

Samples	w (g)	d (mm)	t (mm)	ρ (gcm^{-3})	σ $(\Omega mm)^{-1}$
GM1	0.721	20.187	2.267	0.994	-
GM2	0.723	20.140	2.213	1.025	-
GM3	0.729	20.173	2.243	1.016	-
ACM1	0.316	15.420	1.677	1.008	1.051
ACM2	0.255	14.380	1.470	1.066	0.788
ACM3	0.284	15.233	1.570	0.993	1.111

Figure 1 shows the X-ray diffractograms of the ACMs. All of them indicate that ACMs have turbostratic structure [12-14] with major and minor peaks at ~23.820° and ~44.814° due to diffraction from (002) and (100) planes, respectively. Table 2 shows the calculated values of interlayer spacing (d_{002} and d_{100}) and crystallite dimension (stack height L_c (002)) and stack width L_a (100)) from the diffraction peaks (002) and (100). The relationship between d, L_c surface area and specific capacitance for carbon from EFB is reported in ref. [12].

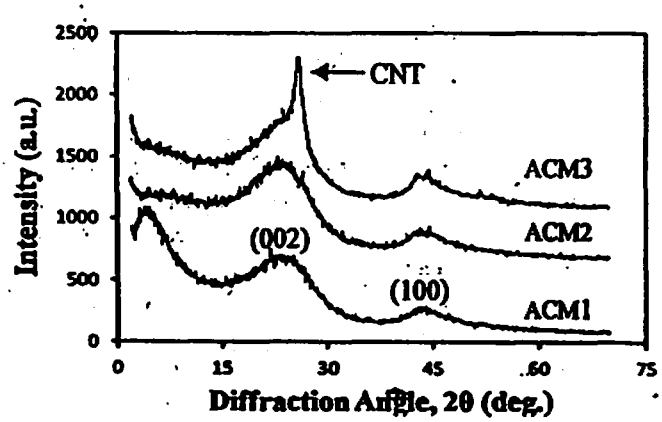

FIGURE 1. X-ray difractograms for ACMs.

TABLE 2. Interlayer spacing and crystallite dimension for ACMs

Samples	d_{002} (Å)	d_{100} (Å)	L_c (Å)	L_a (Å)
ACM1	3.7328	2.0210	10.91	28.79
ACM2	3.8059	2.0252	10.44	32.41
ACM3	3.5721	2.0370	14.12	31.88

Figure 2 shows the plot of adsorption-desorption capacity versus pressure for the ACMs, which have a typical type I isotherm. Table 3 shows the porosity data of the ACMs obtained from the adsorption-desorption

data in Figure 2. The effect of acid treatment appears to reduce the surface area of the ACMs. The addition of CNTs further reduced the surface area of the ACMs.

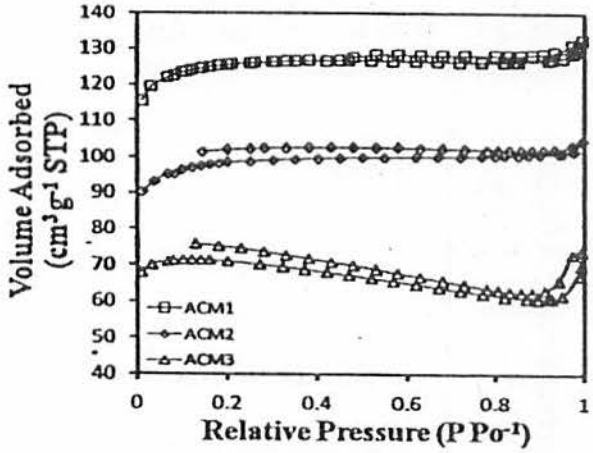

FIGURE 2. Adsorption and desorption of ACMS.

TABLE 3. Porosity data for ACMs

Sample	ACM1	ACM2	ACM3
S_{BET} (m^2g^{-1})	420	329	250
S_{Meso} (m^2g^{-1})	44	40	14
S_{Micro} (m^2g^{-1})	375	290	236
V_{Meso} (cm^3g^{-1})	0.021	0.018	0.007
V_{Micro} (cm^3g^{-1})	0.175	0.135	0.116
D (Å)	19.0	19.2	17.7

Micrographs of FESEM in Figure 3 for the ACMs show the porous microstructure of the samples, with pores evenly distributed throughout the samples. ACM1 seems to be more porous than other samples and the presence of CNTs in some pores can be seen for the ACM3.

The Nyquis plots (i.e. complex impedance plots) from EIS data in Figure 4 show the ACM1 cells have much better capacitive behavior than ACM2 and ACM3 cells. Addition of CNTs seems to make the ACM3 cell have better capacitive behavior than ACM2 cell. All plots (inset a) consist of a semicircle, with intercept at real (Z) axis at R_s for high frequency region and at R_p for lower frequency region. Table 4 shows the values of R_s, R_p, ESR, f_k and R_k of the three cells obtained from the EIS data in Figure 4. R_s is the resistances of electrolyte and contact between current collectors and electrodes, R_p is the internal resistance of electrode, ESR = (R_p-R_s) is the equivalent series resistance, f_k is the knee frequency and R_k is the resistance corresponding to f_k. The specific capacitance was calculated from the EIS data using equation $C_{sp} = 2C_{cell}/m$, where $C_{cell} = -1/(2\pi fZ'')$, f is the frequency (lowest), m is the mass of electrode and Z'' is the imaginary part of impedance (Table 5) [15].

The GCD curves, shown in Figure 5, for the ACMs cells, in the potential range of 0 – 1 V at the current densities of 10 $mAcm^{-2}$, exhibit an almost linear increase (charge) and decrease (discharge) of voltage with time.

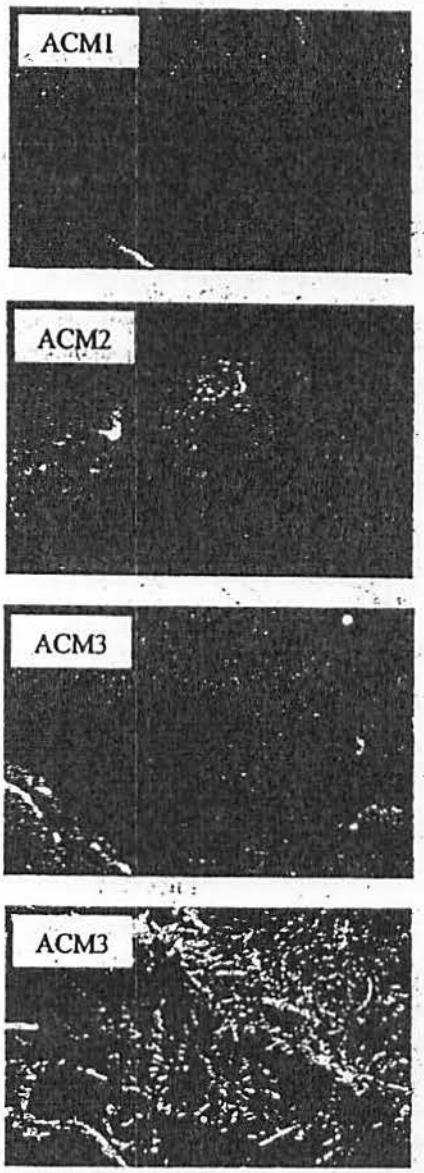

FIGURE 3. FESEM Micrographs for ACMs.

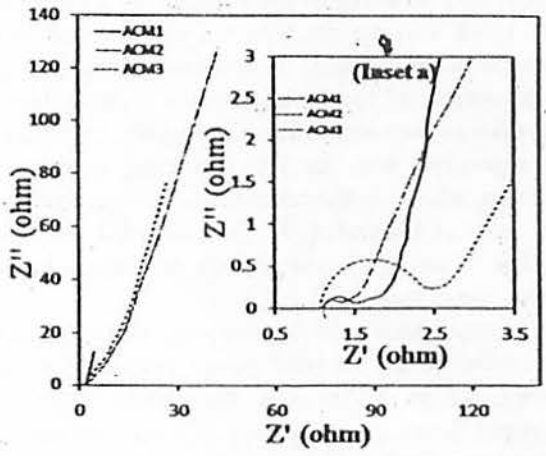

FIGURE 4. Nyquist plots for ACMs cells.

TABLE 4. The values of R_s, R_p, ESR, f_k and R_k for ACM cells

Cells	R_s (Ω)	R_p (Ω)	ESR (Ω)	f_k (Hz)	R_k (Ω)
ACM1	1.116	1.506	0.390	2.512	1.876
ACM2	1.055	2.341	1.286	79.433	2.665
ACM3	1.084	1.335	0.251	79.433	1.547

At the beginning of the discharge curves there is a sharp drop in voltage, which is associated with ESR of the supercapacitor cells. The specific capacitance of the cells were calculated from the discharge curve using equation $C_{sp} = (2I\Delta t)/(m\Delta V)$, where I is the discharge current, Δt is the discharge time, ΔV is the voltage, and m is the mass of electrode [16]. The calculated values of C_{sp}, listed in Table 4, are in agreement with those obtained from the CV and EIS methods.

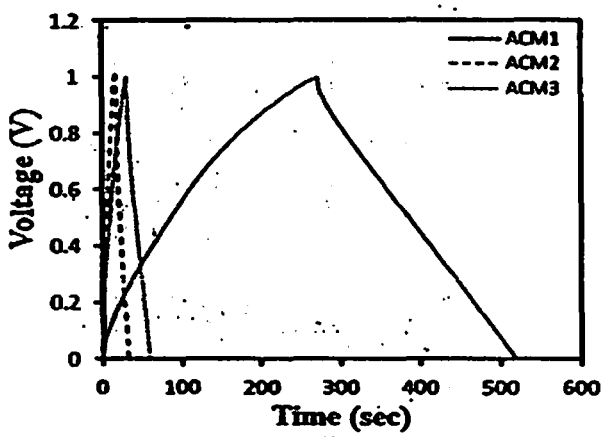

FIGURE 5. GCD curves for ACMs cells.

Figure 6 compares the CV results for the ACMs cells, measured for the potential range from 0.1 V to 1.0 V at a scan rate of 1 mVs^{-1}. The rectangular area represents the capacitive behaviour of the cells; acid treatment reduces such an area, indicating a de-enhancement of the supercapacitive performance of the cells. A slight improvement of the cell performance is observed with the addition CNTs. Another notable feature of the CV curve is that they do not show any evidence for the existance of the redox currents on both the positive and negative sweeps in the potential chosen range. This is a typical characteristic of the supercapacitors using carbon based material as their electrodes. The specific capacitance can be calculated from the CV data using equation $C_{sp} = 2I/(sm)$, where I is the current, s is the scan rate and m is the mass of electrode [17]. The calculated values of C_{sp}, (Table 5) are in agreement with that obtained from the other two methods, EIS and GCD.

Figure 7 shows the Ragone plots which compares the variation of the specific power against the specific energy of the ACMs cells. The values of the specific power (P) and specific energy (E) were calculated from the charge-discharge curves (Figure 5) using equations $P = VI/m$ and $E = VIt/m$, respectively, where I is the discharge current, V is the voltage excluding the iR drop occuring at the beginning of the discharge, t is the time in hour and m is the mass of electrode [18,19,20]. All the cells offer a typical specific power-specific energy relationship. However, the data show a significant decrease in the specific energy due to acid treatment.

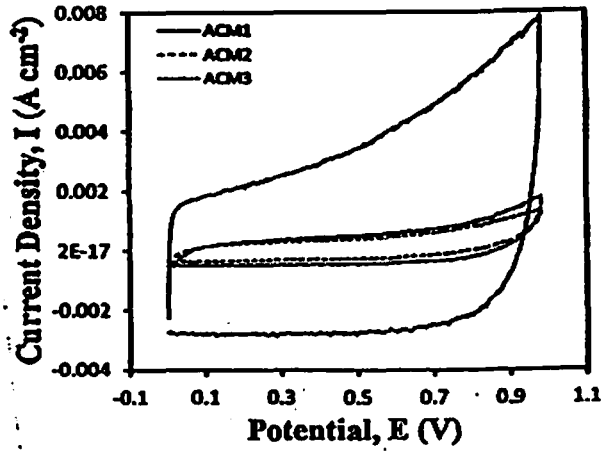

FIGURE 6. CV curves for ACMs cells.

TABLE 5. Specific capacitance (C_{sp}) for ACMs (x = EIS, y = CV, z = GCD)

Cells	$^xC_{sp}$ (Fg^{-1})	$^yC_{sp}$ (Fg^{-1})	$^zC_{sp}$ (Fg^{-1})
ACM1	93.0	85.2	40.7
ACM2	5.7	10.0	4.1
ACM3	10.0	16.7	6.8

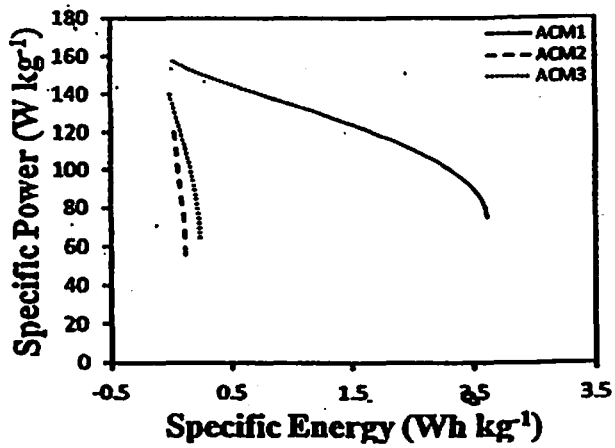

FIGURE 7. Ragone plots for ACMs cells.

Addition of CNTs does not significantly improve the specific energy. A similar effect also observes for the specific power.

CONCLUSION

The ACM from the acid treated GMs from EFB was found to have less mesopores and micropores compared to that from untreated GMs, causing the supercapacitor cells fabricated using these ACM to exhibit a significantly less satisfactory performance. Addition of

CNTs into SACG slightly improved such a less satisfactory performance. These changes associated with the change in the density, electrical conductivity, structure and microstructure of the ACMs. The results of this study suggest that treatment and activation conditions should be changed to obtain a better quality of ACMs.

ACKNOWLEDGMENT

The authors acknowledge the Fundamental Research Grant (UKM-ST-07-FRGS 0030-2009) for the project entitled "Study of Interface between Current Collector and Carbon Electrode Based on Biomass and Nanomaterials in Supercapacitor" and the UKM grant (UKM-OUP-NBT-29-145/2011).

REFERENCES

1. Y. Liu, Z. Hu, K. Xu, X. Zheng, Q. Gao, *Acta Phys. - Chim. Sin.* 24, 1143–1148 (2008).
2. B. Xu, Y. Chen, G. Wei, G. Cao, H. Zhang and Y. Yang, *Mater. Chem. Phys.* 124, 504-509 (2010).
3. R.R. Salunkhe, K. Jang, H. Yu , S. Yu , T. Ganesh, S.-H. Han, H. Ahn, *J. Alloys Compd.* 509, 6677-6682 (2011).
4. V.D. Patake, S.M. Pawar, V.R. Shinde, T.P. Gujar, C.D. Lokhande, *Curr. Appl. Phys.* 10, 99-103 (2010).
5. K.-W. Chang, Z.-Y. Lim, F.-Y. Du, Y.-L. Yang, C.-H. Chang, C.-C. Hu, H.-P. Lin, *Diamond Relat. Mater* 18, 448-451 (2009).
6. G.A. Snook, P. Kao, A.S. Best, *J. Power Sources* 196, 1-12 (2011).
7. P.-L. Taberna, G.C. Chevallier, P. Simon, D. Plee, T. Aubert, *Mater. Res. Bull.* 41, 478-484 (2006).
8. Q.-Y. Li, Z.-S. Li, L. Lin, X.Y. Wang, Y.-F. Wang, C.-H. Zhang, H.-Q. Wang, *Chem.. Eng. J.* 156, 500-504 (2010).
9. C. Li, D. Wang, T. Liang, X.Wang, L.Ji, *Matt. Lett.* 58, 3774-3777 (2004)
10. J.M. Ko, K.M. Kim, *Mater. Chem. Phys.* 114, 837-841 (2009)
11. M. Deraman, R. Omar, and A. G. Harun, *J. Mater. Sci. Lett.*, 17, 2059-2060 (1998).
12. Awitdrus, M. Deraman, I.A. Talib, R. Omar, M.H. Jumali, E. Taer, M.M. Saman, *Sains Malaysiana* 39, 83-86 (2010)
13. A.R. Coutinho, J.D. Rocha, C.A. Luengo, *Fuel Process. Technol.* 67, 93–102 (2000).
14. M. Deraman, S.K.M. Saat, M.M. Ishak, Awitdrus, E. Taer, I.A. Talib, R. Omar, M.H. Jumali, AIP Proceeding, *The 3rd Nanoscience and Nanotechnology Symposium* (NNSB2010), Bandung, Indonesia, 179-186 (2010)
15. E. Taer, M. Deraman, I.A. Talib, A.A. Umar, M. Oyama, R.M. Yunus, *Curr. Appl. Phys.* 10, 1071-1075 (2010)
16. D. Hulicova-Jurcakova, M. Seredych, Y. Jin, G.Q. Lu, T.J. Bandosz, *Carbon* 48, 1767-1778 (2010)
17. A.L.M. Reddy, M.M. Shaijumon, S.R. Gowda, P.M. Ajayan, *J. Phys. Chem.* C 114, 658-663 (2010).
18. E. Taer, M. Deraman, I.A. Talib, S.A. Hashmi, A.A. Umar, *Electrochim. Acta*, 56, 10217-10222 (2011).
19. E. Taer., M. Deraman, I.A. Talib, A. Awitdrus, S.A. Hashmi, A.A. Umar, *Int. J. Electrochem. Sci.* 6, 3301-3315 (2011)
20. A.S. Raut, C.B. Parker, J.T. Glass, *J. Mater. Res.* 25, 1500-1506 (2010).